ACS OMEGA

http://pubs.acs.org/journal/acsodf Article

Spontaneous Movement of a Droplet on a Conical Substrate: Theoretical Analysis of the Driving Force

Jianxin Liu, Zhicheng Feng, Wengen Ouyang, Langquan Shui, and Ze Liu*

Cite This: *ACS Omega* 2022, 7, 20975−20982

Read Online

ACCESS | Metrics & More | Article Recommendations | Supporting Information

ABSTRACT: Experiments and simulations have shown that a droplet can move spontaneously and directionally on a conical substrate. The driving force originating from the gradient of curvatures is revealed as the self-propulsion mechanism. Theoretical analysis of the driving force is highly desirable; currently, most of them are based on a perturbative theory with assuming a weakly curved substrate. However, this assumption is valid only when the size of the droplet is far smaller than the curvature radius of the substrate. In this paper, we derive a more accurate analytical model for describing the driving force by exploring the geometric characteristics of a spherical droplet on a cylindrical substrate. In contrast to the perturbative solution, our model is valid under a much weaker condition, i.e., the contact region between the droplet and the substrate is small compared with the curvature radius of the substrate. Therefore, we show that for superhydrophobic surfaces, the derived analytical model is applicable even if the droplet is very close to the apex of a conical substrate. Our approach opens an avenue for studying the behavior of droplets on the tip of the conical substrate theoretically and could also provide guidance for the experimental design of curved surfaces to control the directional motion of droplets.

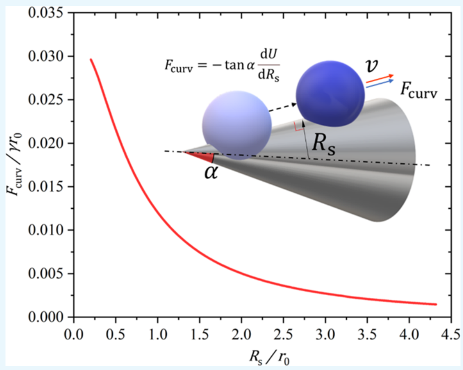

1. INTRODUCTION

The transportation of a droplet has drawn great attention in both academia and industry. Inspired by nature such as the self-cleaning of lotus leaves,[1,2] water or fog collection by spider silk,[3] Namib desert beetles,[4] and cactus,[5] directional water transportation on the peristome surface of *Nepenthes alata*[6] and on the wings of butterfly[7] and cicada,[8] the selectivity for liquid transportation at different surface tensions on Araucaria leaf,[9] and the geometric tip-induced flipping for droplets on the needles of *Sabina chinensis*,[10] a large number of technologies and strategies have been developed for water purification,[11] water collection,[12−16] and controlled transport of droplets.[17,18] The general way to control the directional transport of droplets is by introducing a wettability gradient,[19,20] a roughness gradient,[21,22] or a structure gradient-induced vapor layer gradient.[23] Interestingly, experiments and molecular dynamics (MD) simulations have found that the shape gradient of a substrate typically such as conical substrates can also lead to directional motion of droplets.[24−34] It is believed that the surface free energy gradient is the main driving force in the spontaneous movement of droplets toward the region with a lower curvature.[32−43] In general, the free energy of a droplet−substrate system in a steady state can be quantified as[44] $U = \gamma(A_{LV} - A_{LS}\cos\theta)$, where A_{LV} and A_{LS} denote the contact area of liquid−vapor and liquid−substrate interface, respectively. Therefore, theoretical analysis of the shape gradient-induced driving force requires to accurately calculate the curvature-dependent A_{LV} and A_{LS} since the surface tension of a liquid γ and the contact angle θ[45] are almost constant.[43,46,47] The simplest approximate model to obtain curvature-dependent free energy is to treat both the droplet and the substrate as spheres.[30,39,42] Recently, Galatola[43] and McCarthy et al.[29] investigated the dynamics of a droplet on a conical substrate by performing an approximate calculation of a spherical droplet on a weakly curved cylinder, where the radius of the cylinder corresponds to the local curvature radius of the conical substrate that the droplet is in contact, and the theoretical predictions show agreement with experiments.[14,15,39] However, the analytical solution is based on a perturbative analysis for a substrate close to a plane,[43] and it is applicable only when the radius of the droplet is sufficiently small with respect to that of the substrate so that the variation of the droplet radius is almost independent of the curvature radius of the substrate.

In this work, we theoretically derive the free energy of a droplet on the outside of a conical substrate with consideration of the variation of the droplet radius. The accurate analytical expressions of A_{LV} and A_{LS} for a spherical droplet in contact with a cylindrical substrate are first obtained by exploring the

Received: March 21, 2022
Accepted: May 27, 2022
Published: June 7, 2022

ACS Publications

© 2022 The Authors. Published by American Chemical Society

https://doi.org/10.1021/acsomega.2c01713
ACS Omega 2022, 7, 20975−20982

geometric characteristics. We reveal that the ratio of the liquid−substrate contact size over the radius of the substrate is more suitable to be used as a small quantity in the approximation theory. As a result, by comparison with the Surface Evolver (SE) simulation results, our approximate analytical solutions are valid in a wider range than the previous perturbation method. Especially for superhydrophobic cones, it can effectively predict the behavior of a droplet close to the conical apex. We found that near the conical apex, the curvature-induced driving force increases significantly with the increase in cone angle, while far away from the conical apex, the curvature-induced driving force decreases with the increase in cone angle.

The outline of this paper is as follows: In Section 2, the mathematical model of a droplet on different substrates will be given, and the approximate solutions will be discussed. In Section 3, we will show the system free energy and the curvature-induced driving force and compare them with those obtained by Galatola,[43] Li et al.,[34] and by Lv et al.,[39] and we will show the dynamic behavior of a droplet moving on a conical substrate under the action of the curvature-induced driving force and the resistance force from contact angle hysteresis. Finally, we conclude with a brief summary in Section 4.

2. MATHEMATICAL MODELS

To analytically calculate the curvature-dependent A_{LV} and A_{LS}, there are two approximate models: a spherical droplet on a spherical substrate (S-S model) and a spherical droplet on a cylindrical substrate (S-C model), where the radius of the spherical and the cylindrical substrates corresponds to the local curvature radius of the conical substrate in contact with the droplet. The half-apex angle of the conical substrate is denoted by α.

2.1. A Spherical Droplet on a Spherical Substrate (S-S Model). Considering a spherical droplet on a spherical substrate (S-S model), as shown in Figure 1, the interfacial areas of the liquid−substrate interface and the liquid−vapor interface are

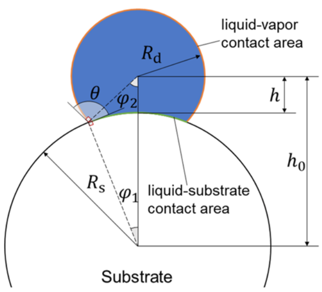

Figure 1. A spherical droplet on a spherical substrate with a contact angle of θ.

$$A_{LS} = \int_0^{\varphi_1} 2\pi R_s^2 \sin\varphi \, d\varphi \tag{1}$$

$$A_{LV} = 4\pi R_d^2 - \int_0^{\varphi_2} 2\pi R_d^2 \sin\varphi \, d\varphi \tag{2}$$

i.e.,

$$A_{LS} = 2\pi R_s^2(1 - \cos\varphi_1) \tag{3}$$

$$A_{LV} = 2\pi R_d^2(1 + \cos\varphi_2) \tag{4}$$

where φ_1 and φ_2 can be determined as

$$\cos\varphi_1 = \frac{R_d^2 + (h + R_s)^2 - R_s^2}{2R_d(h + R_s)} \tag{5}$$

$$\cos\varphi_2 = \frac{R_s^2 + (h + R_s)^2 - R_d^2}{2R_s(h + R_s)} \tag{6}$$

where R_s and R_d are the radii of the substrate and the droplet, respectively, and h is the distance from the center of the droplet to the vertex of the spherical substrate. The parameters of φ_1 and φ_2 as shown in Figure 1 can be determined by minimizing the system free energy, which will be presented in the next section. The volume of the droplet can be calculated as

$$V_d = \frac{4\pi R_d^3}{3} - V_r \tag{7}$$

where $V_r = {}^{\pi}/_{3}(2R_s + h_1)(R_s - h_1)^2 + {}^{\pi}/_{3}(2R_d + h_2)(R_d - h_2)^2$, $h_1 = R_s\cos\varphi_1$, and $h_2 = R_d\cos\varphi_2$. Substituting the above expressions into eqs 3, 4, and 7, we have

$$A_{LS} = \frac{\pi R_s(R_d^2 - h^2)}{h + R_s} \tag{8}$$

$$A_{LV} = \frac{\pi R_d(h + R_d)(h + R_d + 2R_s)}{h + R_s} \tag{9}$$

$$V_d = \frac{\pi(h + R_d)^2}{12(h + R_s)}[3(R_s + R_d)^2 - 2(R_s - R_d)(h + R_s) - (h + R_s)^2] \tag{10}$$

On the other hand, the contact angle θ satisfies

$$\cos\theta = \frac{R_d^2 - h^2 - 2hR_s}{2R_sR_d} \tag{11}$$

2.2. A Spherical Droplet on a Cylindrical Substrate (S-C Model). For the model of a spherical droplet on a cylindrical substrate (Figure 2), the equations of the spherical droplet and the cylindrical substrate in the rectangular coordinate system as shown in Figure 2a are

$$x^2 + y^2 + (z - h_0)^2 = R_d^2 \tag{12}$$

$$x^2 + z^2 = R_s^2 \tag{13}$$

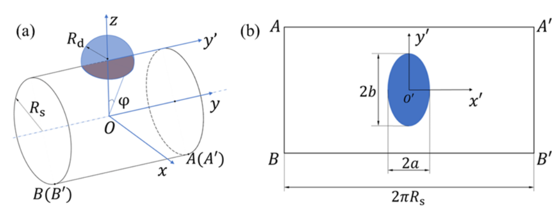

Figure 2. (a) Sketch of a spherical droplet on a cylindrical substrate with a contact angle of θ, where the y-axis is along the axis of the cylindrical substrate and the z-axis goes through the center of the spherical droplet. (b) In the unfolded view along the generatrix AB in (a), the liquid−substrate contact area can be approximated as an ellipse as discussed in the main text.

https://doi.org/10.1021/acsomega.2c01713
ACS Omega 2022, 7, 20975−20982

where h_0 is the distance between the center of the sphere and the axis of the cylinder and R_s and R_d are the radii of the substrate and the droplet, respectively.

Then, the interface areas A_{LS} and A_{LV} read

$$A_{LS} = 4\int_0^{y_1} dy \int_{z_1(y)}^{R_s} \sqrt{\frac{R_s^2}{R_s^2 - z^2}}\, dz \tag{14}$$

and

$$A_{LV} = 4\pi R_d^2 - A_r \tag{15}$$

where

$$y_1 = \sqrt{R_d^2 - (h_0 - R_s)^2} \tag{16}$$

$$z_1(y) = \frac{y^2 + R_s^2 + h_0^2 - R_d^2}{2h_0} \tag{17}$$

$$z_2(y) = h_0 - \sqrt{R_d^2 - y^2} \tag{18}$$

$$A_r = 4\int_0^{y_1} dy \int_{z_2(y)}^{z_1(y)} \sqrt{\frac{R_d^2}{R_d^2 - (z - h_0)^2 - y^2}}\, dz \tag{19}$$

The volume of the droplet can still be formulated using eq 7, and V_r can be calculated as

$$V_r = 4\int_0^{y_1} dy \int_{z_1(y)}^{R_0} dz \int_0^{x_1(y,z)} dx + 4\int_0^{y_1} dy \int_{z_2(y)}^{z_1(y)} dz \int_0^{x_2(y,z)} dx \tag{20}$$

where $x_1(y, z)$ and $x_2(y, z)$ are given by

$$x_1(y, z) = \sqrt{R_d^2 - z^2} \tag{21}$$

$$x_2(y, z) = \sqrt{R_d^2 - y^2 - (z - h_0)^2} \tag{22}$$

2.2.1. Approximate Analytical Solution of the S-C Model. To accurately determine A_{LS} and A_{LV}, numerical integration of eqs 14, 15, and 20 is generally required. However, an approximate analytical solution is highly desired since it is more convenient to guide the experimental design. To obtain the analytical expressions of A_{LS} and A_{LV}, we first derive the equations of the spherical droplet and the cylindrical substrate in the cylindrical coordinate system (Figure 2a):

$$\begin{cases} z = \rho\cos\varphi \\ x = \rho\sin\varphi \\ y = y \end{cases} \tag{23}$$

Then, eqs 12 and 13 can be rewritten as

$$\rho^2 - 2h_0\cos\varphi\cdot\rho + h_0^2 + y^2 = R_d^2 \tag{24}$$

$$\rho = R_s \tag{25}$$

where $h_0 = h + R_s$. The equation of the contact line between the spherical droplet and the cylindrical substrate is thus

$$R_s^2 - 2h_0\cos\varphi\cdot R_s + h_0^2 + y^2 = R_d^2 \tag{26}$$

Taking the Taylor expansion of $\cos\varphi$ as

$$\cos\varphi = 1 - \frac{\varphi^2}{2!} + o(\varphi^2) \tag{27}$$

where $o(\varphi^2)$ can be neglected when φ is very small, then eq 26 can be simplified as

$$R_s^2 - 2h_0R_s + h_0(R_s\varphi^2) + h_0^2 + y^2 = R_d^2 \tag{28}$$

With the definitions of $R_s\varphi = x'$ and $y = y'$, the equation of the contact line can be rewritten as (Figure 2b)

$$\frac{x'^2}{a^2} + \frac{y'^2}{b^2} = 1 \tag{29}$$

where a and b are

$$a = \sqrt{\frac{R_s}{h_0}[(R_s + R_d) - h_0][h_0 - (R_s - R_d)]} \tag{30}$$

$$b = \sqrt{[(R_s + R_d) - h_0][h_0 - (R_s - R_d)]} \tag{31}$$

where $R_s - R_d < h_0 < R_s + R_d$. Based on eq 29, the liquid–substrate interface area A_{LS} can be calculated as

$$A_{LS} = \pi\sqrt{\frac{R_s}{h_0}}(R_d - h_0 + R_s)(R_d + h_0 - R_s) \tag{32}$$

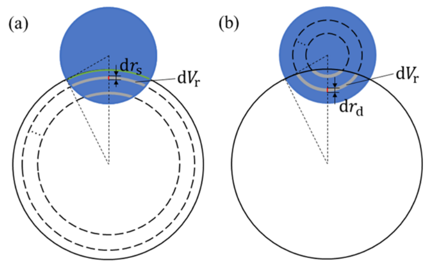

Figure 3. The removed volume of a spherical droplet on a cylinder can be regarded as either the sum of many slices of the sphere cut by cylindrical shells with different radii (a) or as the sum of many slices of the cylinder cut by spherical shells with different radii (b).

Based on eq 32 and dividing V_r with a series of concentric cylindrical surfaces as shown in Figure 3a, dV_r can be readily formulated as

$$dV_r = \pi\sqrt{\frac{r_s}{h_0}}(R_d - h_0 + r_s)(R_d + h_0 - r_s)\, dr_s \tag{33}$$

and

$$V_r = \int_{h_0 - R_d}^{R_s} \pi\sqrt{\frac{r_s}{h_0}}(R_d - h_0 + r_s)(R_d + h_0 - r_s)\, dr_s \tag{34}$$

i.e.,

$$V_r = \frac{2\pi}{105}\left[4(h_0 - R_d)^2(2h_0 + 5R_d)\sqrt{1 - \frac{R_d}{h_0}} - R_s\sqrt{\frac{R_s}{h_0}}(35h_0^2 - 35R_d^2 - 42h_0R_s + 15R_s^2)\right] \tag{35}$$

https://doi.org/10.1021/acsomega.2c01713
ACS Omega 2022, 7, 20975−20982

Based on eqs 7 and 35, the volume of the droplet can be written as

$$V_{\mathrm{d}} = \frac{2\pi R_{\mathrm{s}}^{3}}{105\lambda_{\mathrm{s}}^{6}}(15\lambda_{\mathrm{s}}^{7} + 20\lambda_{\mathrm{d}}^{7} - 70\lambda_{\mathrm{d}}^{6} - 42\lambda_{\mathrm{s}}^{5} - 28\lambda_{\mathrm{d}}^{5} + 210\lambda_{\mathrm{d}}^{4} - 210\lambda_{\mathrm{d}}^{2} - 35\lambda_{\mathrm{s}}^{3}\lambda_{\mathrm{d}}^{4} + 70\lambda_{\mathrm{s}}^{3}\lambda_{\mathrm{d}}^{2} + 70) \tag{36}$$

where $\lambda_{\mathrm{s}} = \sqrt{\frac{R_{\mathrm{s}}}{h_0}}$ and $\lambda_{\mathrm{d}} = \sqrt{1 - \frac{R_{\mathrm{d}}}{h_0}}$.

It is noted that the infinitesimal volume $\mathrm{d}V_{\mathrm{r}}$ can be easily correlated with the liquid−vapor interface area A_{LV} because $A_{\mathrm{LV}} = (4\pi R_{\mathrm{d}}^2 - A_{\mathrm{r}}|_{r_{\mathrm{d}} = R_{\mathrm{d}}})$ and

$$\mathrm{d}V_{\mathrm{r}}(r_{\mathrm{d}}) = A_{\mathrm{r}}(r_{\mathrm{d}})\,\mathrm{d}r_{\mathrm{d}} \tag{37}$$

Based on eqs 33 and 37, we obtain

$$A_{\mathrm{r}}|_{r_{\mathrm{d}}=R_{\mathrm{d}}} = \frac{4}{3}\pi R_{\mathrm{d}}h_0(\lambda_{\mathrm{s}}^{3} - \lambda_{\mathrm{d}}^{3}) \tag{38}$$

Based on eq 15, we obtain

$$A_{\mathrm{LV}} = 4\pi R_{\mathrm{d}}^{2} - \frac{4}{3}\pi R_{\mathrm{d}}h_0(\lambda_{\mathrm{s}}^{3} - \lambda_{\mathrm{d}}^{3}) \tag{39}$$

3. RESULTS AND DISCUSSION

3.1. The System Free Energy of a Spherical Droplet on a Cylindrical Substrate. The system free energy of a liquid droplet on a solid substrate can be quantified as[44]

$$U = \gamma(A_{\mathrm{LV}} - A_{\mathrm{LS}}\cos\theta) \tag{40}$$

The contact angle θ satisfies[45]

$$\cos\theta = \frac{\gamma_{\mathrm{SV}} - \gamma_{\mathrm{LV}}}{\gamma} \tag{41}$$

where γ, γ_{SV}, and γ_{LV} are the liquid−vapor, solid−vapor, and liquid−solid interfacial tension, respectively. When considering the line tension, the system free energy reads

$$U = \gamma A_{\mathrm{LV}} - \gamma A_{\mathrm{LS}}\cos\theta + \tau L \tag{42}$$

where τ is the line tension and L is the perimeter of the solid−liquid contact area. Taking typical values for the spherical droplet on a smooth substrate (without microstructures): $\tau = 10^{-9} - 10^{-6}$ N,[48−50] a liquid radius of >100 μm, a contact angle of 90°, and the surface energy of water $\gamma = 0.072$ N/m, we have $\tau L \leq 6.28 \times (10^{-13} - 10^{-10})$ N·m $\ll (\gamma A_{\mathrm{LV}})|_{\min} = 4.52 \times 10^{-9}$ N·m. Therefore, the line tension effect can be safely neglected on a smooth substrate.

Then, under the conditions of a constant droplet volume and contact angle, h can be determined by minimizing the system free energy

$$\frac{\mathrm{d}U(R_{\mathrm{d}}, h)}{\mathrm{d}h} = 0 \tag{43}$$

i.e.,

$$\frac{\mathrm{d}A_{\mathrm{LV}}(R_{\mathrm{d}}, h)}{\mathrm{d}h} - \cos\theta\,\frac{\mathrm{d}A_{\mathrm{LS}}(R_{\mathrm{d}}, h)}{\mathrm{d}h} = 0 \tag{44}$$

where

$$\frac{\mathrm{d}A_{\mathrm{LV}}(R_{\mathrm{d}}, h)}{\mathrm{d}h} = \frac{\partial A_{\mathrm{LV}}(R_{\mathrm{d}}, h)}{\partial R_{\mathrm{d}}}\cdot\frac{\mathrm{d}R_{\mathrm{d}}(h)}{\mathrm{d}h} + \frac{\partial A_{\mathrm{LV}}(R_{\mathrm{d}}, h)}{\partial h} \tag{45}$$

$$\frac{\mathrm{d}A_{\mathrm{LS}}(R_{\mathrm{d}}, h)}{\mathrm{d}h} = \frac{\partial A_{\mathrm{LS}}(R_{\mathrm{d}}, h)}{\partial R_{\mathrm{d}}}\cdot\frac{\mathrm{d}R_{\mathrm{d}}(h)}{\mathrm{d}h} + \frac{\partial A_{\mathrm{LS}}(R_{\mathrm{d}}, h)}{\partial h} \tag{46}$$

and

$$\frac{\partial A_{\mathrm{LV}}(R_{\mathrm{d}}, h)}{\partial R_{\mathrm{d}}} = \frac{2\pi R_{\mathrm{s}}(5\lambda_{\mathrm{d}}^{3} - 12\lambda_{\mathrm{d}}^{2} - 3\lambda_{\mathrm{d}} - 2\lambda_{\mathrm{s}}^{3} + 12)}{3\lambda_{\mathrm{s}}^{2}} \tag{47}$$

$$\frac{\partial A_{\mathrm{LV}}(R_{\mathrm{d}}, h)}{\partial h} = \frac{2\pi R_{\mathrm{s}}(1 - \lambda_{\mathrm{d}}^{2})(\lambda_{\mathrm{s}}^{3} - \lambda_{\mathrm{d}}^{3} + 3\lambda_{\mathrm{d}})}{3\lambda_{\mathrm{s}}^{2}} \tag{48}$$

$$\frac{\partial A_{\mathrm{LS}}(R_{\mathrm{d}}, h)}{\partial R_{\mathrm{d}}} = \frac{2\pi R_{\mathrm{s}}(1 - \lambda_{\mathrm{d}}^{2})}{\lambda_{\mathrm{s}}} \tag{49}$$

$$\frac{\partial A_{\mathrm{LS}}(R_{\mathrm{d}}, h)}{\partial h} = \frac{\pi R_{\mathrm{s}}(\lambda_{\mathrm{s}}^{4} - 2\lambda_{\mathrm{s}}^{2} - \lambda_{\mathrm{d}}^{4} + 2\lambda_{\mathrm{d}}^{2} - 4)}{2\lambda_{\mathrm{s}}} \tag{50}$$

$$\frac{\mathrm{d}R_{\mathrm{d}}(h)}{\mathrm{d}h} = [15\lambda_{\mathrm{s}}^{7} + 42\lambda_{\mathrm{s}}^{5} - 35\lambda_{\mathrm{s}}^{3}(\lambda_{\mathrm{d}}^{4} - 2\lambda_{\mathrm{d}}^{2} + 4) + 4\lambda_{\mathrm{d}}^{3}(5\lambda_{\mathrm{d}}^{4} - 28\lambda_{\mathrm{d}}^{2} + 35)]/[140(1 - \lambda_{\mathrm{d}}^{2})(\lambda_{\mathrm{d}}^{3} - 3\lambda_{\mathrm{d}}^{2} - \lambda_{\mathrm{s}}^{3} + 3)] \tag{51}$$

The system free energy can thus be calculated by solving eqs 7 and 44 under the condition of

$$R_{\mathrm{d}} > |h| > 0 \tag{52}$$

If the contact size between a droplet and a conical substrate is small by comparison with the local curvature radius of the conical substrate, then the free energy of a droplet−conical substrate system can be approximated by that of a droplet−cylindrical substrate system with the radius of (Figure 4)

$$R_{\mathrm{s}} = \tan\alpha\cdot s \tag{53}$$

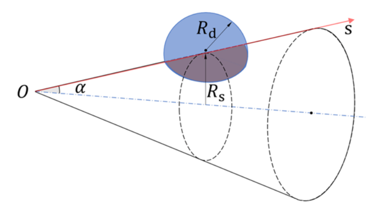

Figure 4. The model of a spherical droplet on a conical substrate with a half-apex angle α.

where s is the coordinate along the generatrix of the conical substrate. Then, by substituting eqs 32 and 39 into eq 40, we obtain the system free energy of a droplet on a conical substrate as

$$U = \gamma\pi\left[4R_{\mathrm{d}}^{2} - \frac{4}{3}R_{\mathrm{d}}(h + R_{\mathrm{s}})(\lambda_{\mathrm{s}}^{3} - \lambda_{\mathrm{d}}^{3}) - \lambda_{\mathrm{s}}(R_{\mathrm{d}}^{2} - h^{2})\cos\theta\right] \tag{54}$$

For simplicity, we introduce the nominal radius of the droplet as $r_0 = \left(\frac{3}{4\pi}V_{\mathrm{d}}\right)^{1/3}$ and then define the dimensionless system free energy and the local radius of R_{s} as $U^* = U/\gamma r_0^2$ and $R_{\mathrm{s}}^* = R_{\mathrm{s}}/r_0$, respectively. The dimensionless free energy of a

https://doi.org/10.1021/acsomega.2c01713
ACS Omega 2022, 7, 20975−20982

droplet on a conical substrate is plotted in Figure 5, where the perturbative solution to the S-C model by Galatola (hereafter abbreviated as "Galatola's approximation")[43] is also shown for comparison. It is obvious that the S-S model shows a consistent trend by comparison with the exact numerical solution of the S-C model, but there is a large deviation for the S-S model in ref 39 and the Galatola's approximation[43] (the double dot-dashed line and the green dotted line in Figure 5), where Galatola's approximation shows good agreement at a large radii (corresponding to a weakly curved cylinder) but considerable deviation exists at small R_s^* values, while our approximate analytical solution (eq 54) agrees very well with the exact numerical solution in the entire range of R_s^* (red solid line in Figure 5).

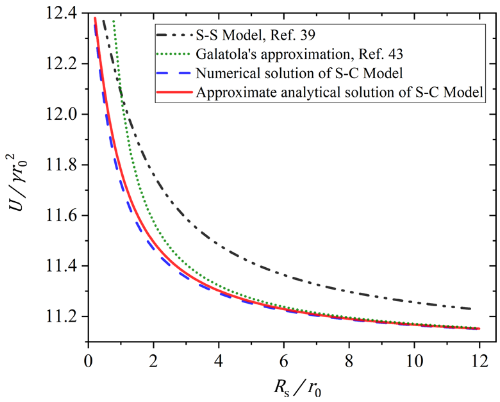

Figure 5. The dimensionless system free energy $U/\gamma r_0^2$ versus the dimensionless local radius R_s/r_0 of the conical substrate. The double dot-dashed line is the approximate solution in ref 39. The green dotted line is the result based on Galatola's approximation.[43] The blue dashed line is the numerical solution of the S-C model, and the red solid line is the approximate analytical solution of the S-C model based on eq 54. The contact angle of $\cos\theta = -0.25$ and the volume of the droplet V_d = 30 mm^3 are used in the calculations.

Based on eqs 53 and 54, the curvature gradient-induced driving force F_{curv} can be readily calculated by

$$F_{curv} = -\frac{dU}{ds} = -\tan\alpha \frac{dU}{dR_s} \tag{55}$$

Defining the dimensionless curvature gradient as $F_{curv}^* = F_{curv}/\gamma r_0$, we have

$$F_{curv}^* = -\tan\alpha \frac{dU^*}{dR_s^*} \tag{56}$$

The curvature gradient-induced force, F_{curv}^*, is plotted in Figure 6, where the results obtained by the S-S model,[39] perturbative analytical solution,[43] and the Surface Evolver (SE) simulation in ref 34 are also shown for comparison. To compare with the literatures, the contact angle θ in Figure 6a is varied form $\theta = 90°$ to $\theta = 120°$, and the half-apex angle of the conical substrate α is 19.5°,[39] where the blue dashed lines are taken from ref 39. It is clear that both the S-S model and our approximate S-C model show similar trends on R_s/r_0, that is, the curvature-induced force decreases drastically with the increase in R_s/r_0 and tends to zero at positions far away from the apex, but significant deviation can appear at small R_s/r_0 values. Similarly, by comparison with the perturbative analytical solution (black dashed line in Figure 6b),[43] our approximate analytical solution (red line in Figure 6b) shows much better agreement with the SE simulation results[34] (blue dashed line in Figure 6b). The curvature-induced force decreases with increasing R_s/r_0 and tends to 0 on the position far away from the apex.

In addition, when plotting the dimensionless curvature gradient-induced force F_{curv}^* versus the dimensionless coordinate s/r_0 (i.e., along the generatrix of the conical substrate) with a varied half-apex angle α (Figure 7), we observed that the driving force decreases drastically as s/r_0 increases, and the smaller the θ, the higher the driving force, which agrees well with MD simulations.[38,39] Remarkably, our model also predicts that far away from the conical apex, the driving force decreases as α increases, but near the conical apex, the driving force drastically grows as α increases. Such a prediction suggests that a larger apex angle can lead to a faster water collection speed near the conical apex, which is consistent with experimental observation.[14,15,39] It is noteworthy that our approximate formula is valid as long as the size of the liquid−solid contact area is small by comparison with the curvature radius of the substrate. Therefore, our approximation method can predict the behavior of a droplet in the region very close to the conical apex in the hydrophobic (superhydrophobic) case. This is very

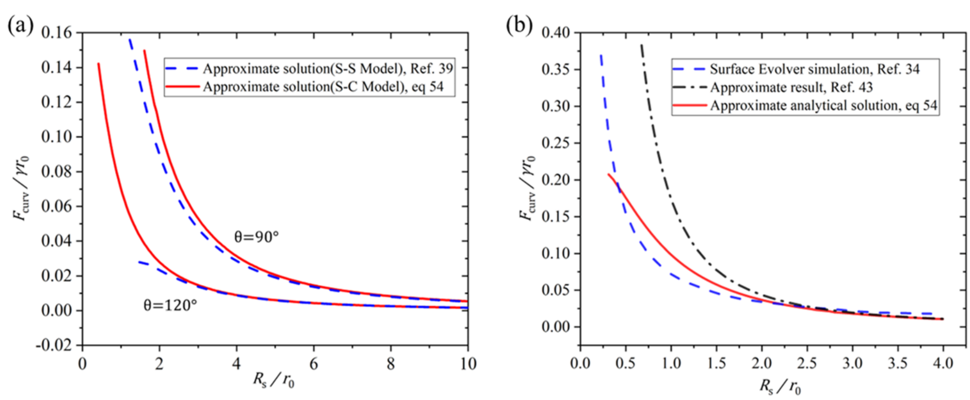

Figure 6. The dimensionless curvature gradient-induced force F_{curv}^* versus the dimensionless local radius R_s/r_0 of a conical substrate. (a) Conical substrate with a half-apex angle α = 19.5°. The red solid lines are calculated based on eq 54, and the blue dashed lines are the results based on the S-S model in ref 39. (b) Conical substrate with a half-apex angle α = 5° and a contact angle θ = 80°; the volume of the droplet V_d = 30 mm^3 is used. The blue dashed line is obtained by the Surface Evolver simulation in ref 34, the black dot-dashed line is the approximation result from ref 43, and the red solid line is our calculation based on eq 54.

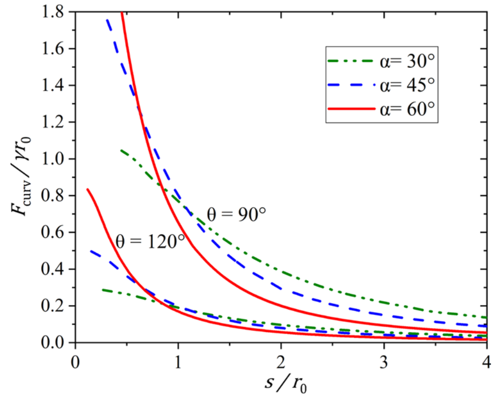

Figure 7. The curvature gradient-induced force F^*_{curv} versus the coordinate s along the generatrix of conical substrates with different half-apex angles (α = 30 (green double dot − dashed line),45 (blue dashed line), and 60° (red solid line)), where the contact angle and the volume of the droplet are set as θ = 90 and 120° and V_d = 30 mm^3, respectively.

different from the perturbative approximation method, typically such as Galatola's approximation,[43] which is derived based on the condition that the droplet radius is far smaller than the curvature radius of the substrate. In other words, even in the case of superhydrophobic with an almost zero contact area, if the droplet is large, then the perturbative approximation method will fail even at the region far away from the apex of a conical substrate.

3.2. Dynamic Analysis of the Motion of a Droplet on a Conical Substrate.

When a droplet moves on a conical substrate, it suffers from both the curvature gradient-induced driving force (eq 55) and the resistance force from the contact angle hysteresis (F_h)[51]

$$F_h = \gamma wk(\cos\theta_r - \cos\theta_a) \tag{57}$$

where θ_a and θ_r are the advancing and receding contact angles, respectively, and w is a characteristic length of the contact area, where for the elliptical contact interface shown in Figure 2b, $w = a$, i.e.,

$$w = \lambda_s\sqrt{{R_d}^2 - h^2} \tag{58}$$

and

$$k = -\frac{2}{\pi}\int_0^{\pi} t\cos t\,(\beta^2\cos^2 t + \sin^2 t)^{1/2}\,dt \tag{59}$$

where $\beta = b/a = \lambda_s^{-1}$. The resultant force on the droplet is thus $F_a = F_{curv} - F_h$. Then, the equation of motion of the droplet in the steady state reads

$$F_a = \rho V_d v\frac{dv}{ds} \tag{60}$$

where ρ is the density of the liquid and v is the velocity of the droplet. Integration of eq 60 gives

$$v^2 = \int\frac{2F_a}{\rho V_d}\,ds \tag{61}$$

Substituting eq 53 into eq 61 gives

$$v^2 = \int\frac{2F_a}{\rho V_d\tan\alpha}\,dR_s \tag{62}$$

Based on eq 62, the velocity v of the droplet versus the generatrix of the conical substrate can be obtained (Figure 8).

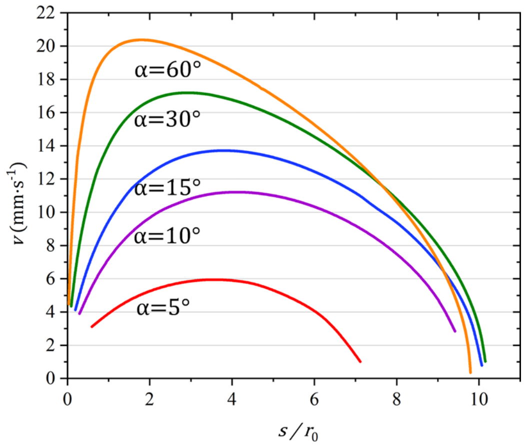

Figure 8. The stead-state velocity v of a droplet moving along the generatrix of conical substrates with half-apex angles of α = 5,10,15,30, and 60°, where the contact angle and the volume of the droplet are set as θ = 90° and V_d = 30 mm^3, respectively. The advancing and receding contact angles are θ_a = 95° and θ_r = 85°, respectively. The liquid−solid interface tension is γ = 1 N/m, and the density of the liquid is $\rho = 1.0 \times 10^3$ kg/m^3.

It is observed that the velocity of a droplet on a conical substrate increases first and then decreases and finally goes to zero as the distance from the conical apex increases, and the larger the half-apex angle, the faster the average velocity of the directional movement of a droplet on a conical substrate. This prediction also agrees well with the experimental observations by Gurera and Bhushan.[14,15]

4. CONCLUSIONS

In summary, we present a theoretical model for describing the curvature gradient-induced directional motion of a droplet on a conical substrate. By exploring the geometric characteristics of a sphere droplet on a cylindrical substrate and formulating the contact interface area of the liquid−substrate and the liquid−vapor, we derived a new approximate analytical expression of the system free energy and the curvature gradient-induced driving force. By comparison with the approximate analytical solution based on the perturbation method,[43] our analytical solution shows much better agreement with the exact numerical solution, which we attributed to the fact that our method only requires that the contact size of the droplet−solid substrate is smaller than the curvature radius of the substrate, which is much weaker than the condition required by the used perturbation method in the literature. We further show that our theoretical calculations agree well with the results obtained by the Surface Evolver (SE) simulations,[34] the molecular dynamics simulations,[38,39] and experimental observations.[14,15,39] Considering that the developed new analytical model is valid at the region close to the apex of a conical substrate, especially for superhydrophobic substrates, we anticipate that our method should provide a simple but practical guide to experimental design of curved surfaces for studying and controlling the directional motion of droplets.

https://doi.org/10.1021/acsomega.2c01713
ACS Omega 2022, 7, 20975−20982

ASSOCIATED CONTENT

Supporting Information

The Supporting Information is available free of charge at https://pubs.acs.org/doi/10.1021/acsomega.2c01713.

Detailed derivation of the elliptic equation in the unfolded view of the S-C model and details of the relationship between the local radius and the coordinate along the generatrix of the conical substrate (PDF)

AUTHOR INFORMATION

Corresponding Author

Ze Liu − *Department of Engineering Mechanics, School of Civil Engineering, Wuhan University, Wuhan, Hubei 430072, China;* orcid.org/0000-0002-9906-5351; Email: ze.liu@whu.edu.cn

Authors

Jianxin Liu − *Department of Engineering Mechanics, School of Civil Engineering, Wuhan University, Wuhan, Hubei 430072, China*

Zhicheng Feng − *Department of Engineering Mechanics, School of Civil Engineering, Wuhan University, Wuhan, Hubei 430072, China*

Wengen Ouyang − *Department of Engineering Mechanics, School of Civil Engineering, Wuhan University, Wuhan, Hubei 430072, China;* orcid.org/0000-0001-8700-1978

Langquan Shui − *Department of Engineering Mechanics, School of Civil Engineering, Wuhan University, Wuhan, Hubei 430072, China;* orcid.org/0000-0002-5079-9629

Complete contact information is available at: https://pubs.acs.org/10.1021/acsomega.2c01713

Notes

The authors declare no competing financial interest.

ACKNOWLEDGMENTS

This work is supported by the Key Research and Development Program of Hubei Province (2021BAA192) and the Wuhan University Student Innovation Project.

REFERENCES

(1) Cheng, Y. T.; Rodak, D. E.; Wong, C. A.; Hayden, C. A. Effects of micro- and nano-structures on the self-cleaning behaviour of lotus leaves. *Nanotechnology* **2006**, *17*, 1359−1362.

(2) Zhang, M.; Feng, S.; Wang, L.; Zheng, Y. Lotus effect in wetting and self-cleaning. *Biotribology* **2016**, *5*, 31−43.

(3) Zheng, Y.; Bai, H.; Huang, Z.; Tian, X.; Nie, F. Q.; Zhao, Y.; Zhai, J.; Jiang, L. Directional water collection on wetted spider silk. *Nature* **2010**, *463*, 640−643.

(4) Parker, A. R.; Lawrence, C. R. Water capture by a desert beetle. *Nature* **2001**, *414*, 33−34.

(5) Ju, J.; Bai, H.; Zheng, Y.; Zhao, T.; Fang, R.; Jiang, L. A multi-structural and multi-functional integrated fog collection system in cactus. *Nat. Commun.* **2012**, *3*, 1247.

(6) Chen, H.; Zhang, P.; Zhang, L.; Liu, H.; Jiang, Y.; Zhang, D.; Han, Z.; Jiang, L. Continuous directional water transport on the peristome surface of *Nepenthes alata*. *Nature* **2016**, *532*, 85−89.

(7) Zheng, Y.; Gao, X.; Jiang, L. Directional adhesion of superhydrophobic butterfly wings. *Soft Matter* **2007**, *3*, 178−182.

(8) Lee, W.; Jin, M.-K.; Yoo, W.-C.; Lee, J.-K. Nanostructuring of a polymeric substrate with well-defined nanometer-scale topography and tailored surface wettability. *Langmuir* **2004**, *20*, 7665−7669.

(9) Feng, S.; Zhu, P.; Zheng, H.; Zhan, H.; Chen, C.; Li, J.; Wang, L.; Yao, X.; Liu, Y.; Wang, Z. Three-dimensional capillary ratchet-induced liquid directional steering. *Science* **2021**, *373*, 1344−1348.

(10) Feng, S.; Delannoy, J.; Malod, A.; Zheng, H.; Quéré, D.; Wang, Z. Tip-induced flipping of droplets on Janus pillars: From local reconfiguration to global transport. *Sci. Adv.* **2020**, *6*, No. eabb4540.

(11) Brown, P. S.; Bhushan, B. Bioinspired materials for water supply and management: water collection, water purification and separation of water from oil. *Philos. Trans. R. Soc., A* **2016**, *374*, 20160135.

(12) Andrews, H. G.; Eccles, E. A.; Schofield, W. C. E.; Badyal, J. P. S. Three-dimensional hierarchical structures for fog harvesting. *Langmuir* **2011**, *27*, 3798−3802.

(13) Pinchasik, B. E.; Kappl, M.; Butt, H. J. Small Structures, Big Droplets: The Role of Nanoscience in Fog Harvesting. *ACS Nano* **2016**, *10*, 10627−10630.

(14) Gurera, D.; Bhushan, B. Designing bioinspired surfaces for water collection from fog. *Philos. Trans. R. Soc., A* **2019**, *377*, 20180269.

(15) Gurera, D.; Bhushan, B. Optimization of bioinspired conical surfaces for water collection from fog. *J. Colloid Interface Sci.* **2019**, *551*, 26−38.

(16) Xu, T.; Lin, Y.; Zhang, M.; Shi, W.; Zheng, Y. High-Efficiency Fog Collector: Water Unidirectional Transport on Heterogeneous Rough Conical Wires. *ACS Nano* **2016**, *10*, 10681−10688.

(17) Comanns, P.; Buchberger, G.; Buchsbaum, A.; Baumgartner, R.; Kogler, A.; Bauer, S.; Baumgartner, W. Directional, passive liquid transport: the Texas horned lizard as a model for a biomimetic 'liquid diode'. *J. R. Soc., Interface* **2015**, *12*, 20150415.

(18) Dudukovic, N. A.; Fong, E. J.; Gemeda, H. B.; DeOtte, J. R.; Cerón, M. R.; Moran, B. D.; Davis, J. T.; Baker, S. E.; Duoss, E. B. Cellular fluidics. *Nature* **2021**, *595*, 58−65.

(19) Zamuruyev, K. O.; Bardaweel, H. K.; Carron, C. J.; Kenyon, N. J.; Brand, O.; Delplanque, J. P.; Davis, C. E. Continuous droplet removal upon dropwise condensation of humid air on a hydrophobic micropatterned surface. *Langmuir* **2014**, *30*, 10133−10142.

(20) Liu, C.; Sun, J.; Li, J.; Xiang, C.; Che, L.; Wang, Z.; Zhou, X. Long-range spontaneous droplet self-propulsion on wettability gradient surfaces. *Sci. Rep.* **2017**, *7*, 7552.

(21) Sun, C.; Zhao, X.-W.; Han, Y.-H.; Gu, Z.-Z. Control of water droplet motion by alteration of roughness gradient on silicon wafer by laser surface treatment. *Thin Solid Films* **2008**, *516*, 4059−4063.

(22) Moradi, N.; Varnik, F.; Steinbach, I. Roughness-gradient-induced spontaneous motion of droplets on hydrophobic surfaces: A lattice Boltzmann study. *EPL* **2010**, *89*, 26006.

(23) Li, J.; Hou, Y.; Liu, Y.; Hao, C.; Li, M.; Chaudhury, M. K.; Yao, S.; Wang, Z. Directional transport of high-temperature Janus droplets mediated by structural topography. *Nat. Phys.* **2016**, *12*, 606−612.

(24) Li, J.; Guo, Z. Spontaneous directional transportations of water droplets on surfaces driven by gradient structures. *Nanoscale* **2018**, *10*, 13814−13831.

(25) Zhang, J.; Han, Y. Shape-gradient composite surfaces: water droplets move uphill. *Langmuir* **2007**, *23*, 6136−6141.

(26) Yin, Y.-j.; Wu, J. Shape gradient: A driving force induced by space curvatures. *Int. J. Nonlinear Sci. Numer. Simul.* **2010**, *11*, 259−268.

(27) Yin, Y.-j.; Chen, C.; Lü, C.-j.; Zheng, Q.-s. Shape gradient and classical gradient of curvatures: driving forces on micro/nano curved surfaces. *Appl. Math. Mech., Engl. Ed.* **2011**, *32*, 533−550.

(28) Heng, X.; Luo, C. Liquid drop runs upward between two nonparallel plates. *Langmuir* **2015**, *31*, 2743−2748.

(29) McCarthy, J.; Vella, D.; Castrejón-Pita, A. A. Dynamics of droplets on cones: self-propulsion due to curvature gradients. *Soft Matter* **2019**, *15*, 9997−10004.

(30) Chen, Y.; Xu, X. Self-propulsion dynamics of small droplets on general surfaces with curvature gradient. *Phys. Fluids* **2021**, *33*, No. 082107.

(31) Xiao, X.; Li, S.; Zhu, X.; Xiao, X.; Zhang, C.; Jiang, F.; Yu, C.; Jiang, L. Bioinspired Two-Dimensional Structure with Asymmetric

Wettability Barriers for Unidirectional and Long-Distance Gas Bubble Delivery Underwater. *Nano Lett.* **2021**, *21*, 2117−2123.
(32) Lorenceau, L.; Quéré, D. Drops on a conical wire. *J. Fluid Mech.* **1999**, *510*, 29−45.
(33) Liu, J.-L.; Xia, R.; Li, B.-W.; Feng, X.-Q. Directional motion of droplets in a conical tube or on a conical fibre. *Chin. Phys. Lett.* **2007**, *24*, 3210.
(34) Li, Y.; Wu, H.; Wang, F. Stagnation of a droplet on a conical substrate determined by the critical curvature ratio. *J. Phys. D: Appl. Phys.* **2016**, *49*, No. 085304.
(35) Mahmood, A.; Chen, S.; Chen, C.; Weng, D.; Wang, J. Directional Motion of Water Droplet on Nanocone Surface Driven by Curvature Gradient: A Molecular Dynamics Simulation Study. *J. Phys. Chem. C* **2018**, *122*, 14937−14944.
(36) Chan, T. S.; Yang, F.; Carlson, A. Directional spreading of a viscous droplet on a conical fibre. *J. Fluid Mech.* **2020**, 894.
(37) Liang, Y. E.; Tsao, H. K.; Sheng, Y. J. Drops on hydrophilic conical fibers: gravity effect and coexistent states. *Langmuir* **2015**, *31*, 1704−1710.
(38) Lv, C.; Chen, C.; Yin, Y.; Zheng, Q., Surface curvature-induced directional movement of water droplets. *arXiv (Physics.Classical Physics)*, 2010, 1011.3689.
(39) Lv, C.; Chen, C.; Chuang, Y. C.; Tseng, F. G.; Yin, Y.; Grey, F.; Zheng, Q. Substrate curvature gradient drives rapid droplet motion. *Phys. Rev. Lett.* **2014**, *113*, No. 026101.
(40) Schriner, C. T.; Bhushan, B. Water droplet dynamics on bioinspired conical surfaces. *Philos. Trans. R. Soc., A* **2019**, *377*, 20190118.
(41) Michielsen, S.; Zhang, J.; Du, J.; Lee, H. J. Gibbs free energy of liquid drops on conical fibers. *Langmuir* **2011**, *27*, 11867−11872.
(42) Chuang, Y.; Hsieh, H.; Zheng, Q.; Tseng, F.-G. Spontaneous motion of a water droplet on hydrophilic and curvature gradient conical-shaped surfaces. In *2012 7th IEEE International Conference on Nano/Micro Engineered and Molecular Systems*; IEEE, 2012; pp. 403−406.
(43) Galatola, P. Spontaneous capillary propulsion of liquid droplets on substrates with nonuniform curvature. *Phys. Rev. Fluids* **2018**, *3*, 103610.
(44) de Gennes, P. G. Wetting: statics and dynamics. *Rev. Mod. Phys.* **1985**, *57*, 827−863.
(45) Young, T. III. An essay on the cohesion of fluids. *Philos. Trans. R. Soc. London* **1805**, *95*, 65−87.
(46) Vafaei, S.; Podowski, M. Z. Analysis of the relationship between liquid droplet size and contact angle. *Adv. Colloid Interface Sci.* **2005**, *113*, 133−146.
(47) Lu, Z.; Ng, T. W.; Yu, Y. Fast modeling of clam-shell drop morphologies on cylindrical surfaces. *Int. J. Heat Mass Transfer* **2016**, *93*, 1132−1136.
(48) Zheng, Q.; Lv, C.; Hao, P.; Sheridan, J. Small is beautiful, and dry. *Sci. China: Phys. Mech. Astron.* **2010**, *53*, 2245−2259.
(49) Amirfazli, A.; Neumann, A. W. Status of the three-phase line tension: a review. *Adv. Colloid Interface Sci.* **2004**, *110*, 121−141.
(50) Fan, H. Liquid droplet spreading with line tension effect. *J. Phys.: Condens. Matter* **2006**, *18*, 4481.
(51) Extrand, C. W.; Kumagai, Y. Liquid drops on an inclined plane: the relation between contact angles, drop shape, and retentive force. *J. Colloid Interface Sci.* **1995**, *170*, 515−521.

https://doi.org/10.1021/acsomega.2c01713
ACS Omega 2022, 7, 20975−20982